ACS Photonics

Article

Cite This: ACS Photonics 2019, 6, 787−792

pubs.acs.org/journal/apchd5

Plasmon-Resonant Enhancement of Photocatalysis on Monolayer WSe_2

Jihan Chen,[†] Connor S. Bailey,[‡] Yilun Hong,[§,∥] Li Wang,[⊥] Zhi Cai,[#] Lang Shen,[#] Bingya Hou,[†] Yu Wang,[#] Haotian Shi,[○] Justin Sambur,[⊥] Wencai Ren,[§,∥] Eric Pop,[‡] and Stephen B. Cronin*[,†,○,□]

[†]Ming Hsieh Department of Electrical Engineering, [#]Mork Family Department of Chemical Engineering and Materials Science, [○]Department of Chemistry, and [□]Department of Physics and Astronomy, University of Southern California, Los Angeles, California 90089, United States

[‡]Department of Electrical Engineering, Stanford University, Stanford, California 94305, United States

[§]Shenyang National Laboratory for Materials Science, Institute of Metal Research, Chinese Academy of Sciences, Shenyang, 110016, People's Republic of China

[∥]School of Materials Science and Engineering, University of Science and Technology of China, 72 Wenhua Road, Shenyang, 110016, People's Republic of China

[⊥]Department of Chemistry, Colorado State University, Fort Collins, Colorado 80523, United States

Supporting Information

ABSTRACT: We report plasmonic enhancement of photocatalysis by depositing 5 nm Au nanoislands onto tungsten diselenide (WSe_2) monolayer films. Under 532 nm wavelength illumination, the bare WSe_2 film produces a relatively small photocurrent (20 nA). With the addition of Au nanoparticles, we observe enhancements of up to 7× (0.14 μA) in the measured photocurrent. Despite these relatively small photocurrents, it is remarkable that adequate charge separating fields are generated over just 7.3 Å of material. Here, the improvement in the photocatalytic performance is caused by the local electric field enhancement produced in the monolayer WSe_2 monolayer by the plasmonic Au nanoislands, as verified by electromagnetic simulations using the finite different time domain (FDTD) method. The near-field optical enhancement increases the electron−hole pair generation rate at the surface of WSe_2, thus, increasing the amount of photogenerated charge contributing to photoelectrochemical reactions. Despite reducing the effective surface area of WSe_2 in contact with the electrolytic solution by 70%, the plasmonic nanoislands couple the incident light very effectively from the far field to the near field in the plane of the monolayer WSe_2, thereby improving the overall photoconversion efficiency from 3.5% to 24.7%.

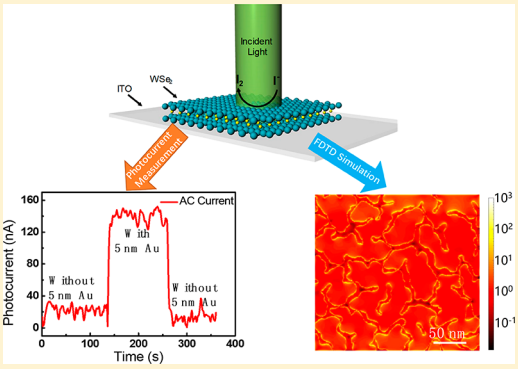

KEYWORDS: *plasmon, photocatalysis, tungsten diselenide, water splitting, enhancement, FDTD, TMDC*

The production of hydrogen and other fuels from photocatalysis has attracted considerable attention as a potential means of generating and storing energy from sunlight. This approach can provide renewable energy in a clean and environmentally friendly manner without utilizing fossil fuels or emitting carbon dioxide.[1−5] Over 100 semiconductor materials, including ZnO, GaN, WO_3, and $BiVO_4$, have already been identified as suitable candidates for solar energy conversion after the first demonstration of photocatalytic splitting of water under ultraviolet radiation on TiO_2 electrodes by Fujishima and Honda in 1972.[6−12] However, many challenges remain in the improvement of quantum efficiencies, promotion of charge transfer at interfaces, increasing activation of catalysts, and suppression of backward reactions involving shuttle redox mediators.[13−16]

The transition metal dichalcogenide (TMDC) family of two-dimensional (2D) materials have high surface-to-volume ratios and exhibit a wide range of interesting electronic and optical properties that stand in contrast to most known bulk materials. These properties include large exciton binding energies, which are stable at room temperature and directly affect a material's ability to function as a photocatalyst. Their high surface-to-volume ratios provide large available surface area for photocatalytic activities and reduces the distance from photogenerated carriers to the solid/water interface. This large surface-to-volume ratio, on the other hand, can increase nonradiative recombination substantially, which is detrimental to photocatalytic performance, presenting a trade-off in the overall photocatalytic performance that is yet to be fully explored. The TMDC materials also offer band gaps spanning a wide range from the near-infrared through the visible and

Received: January 17, 2019
Published: February 19, 2019

DOI: 10.1021/acsphotonics.9b00089
ACS Photonics 2019, 6, 787−792

ultraviolet wavelength ranges to make full use of the entire solar spectrum.[16,17]

Utilization of 2D materials as photocatalysts has been shown to exceed the photocatalytic performance compared to their bulk material counterparts. Sun et al. reported an all-surface-atomic SnS sheet-based photoelectrode exhibiting a 67.1% incident photon-to-current conversion efficiency at 490 nm, which is strikingly higher than that of the bulk counterpart which is only 1.66%. Under visible wavelength illumination, the photocurrent density of the all-surface-atomic SnS sheet-based photoelectrode could reach a value up to 5.27 mA·cm^{-2}, which is 2 orders of magnitude higher than that of the corresponding bulk material.[18] Looking strictly at the electrocatalytic properties of WS_2 (rather than the photocatalytic properties), Voiry et al. has shown that monolayer nanosheets of chemically exfoliated WS_2 are efficient catalysts for hydrogen evolution under very low overpotentials. Here, the enhanced electrocatalytic activity of WS_2 was attributed to the high concentration of the strained metallic octahedral phase in the as-exfoliated nanosheets.[19] Liang et al. reported 3 nm thick free-floating SnO sheets (~6 layers thick) synthesized via a liquid exfoliation strategy showing an incident photon-to-current conversion efficiency of up to 20.1% at 300 nm, remarkably higher than 10.7% and 4.2% for the 5.4 nm thick SnO (~11 layers thick) sheet-based and bulk SnO-based photoelectrodes.[20]

In this work, we demonstrate enhanced photocatalysis using high-quality monolayer WSe_2 grown by chemical vapor deposition (CVD), as shown in the optical microscope image of Figure 1a. This monolayer material exhibits strong photoluminescence (PL) with direct band gap emission around 1.63 eV, as shown in Figure 1b. In addition, we integrate plasmon resonant nanostructures with this photocatalytic semiconductor, which is an approach that has gained considerable attention in the fields of photocatalytic water splitting,[21,22] water purification,[23,24] and CO_2 reduction,[25] as well as dye-sensitized solar cells.[26,27]

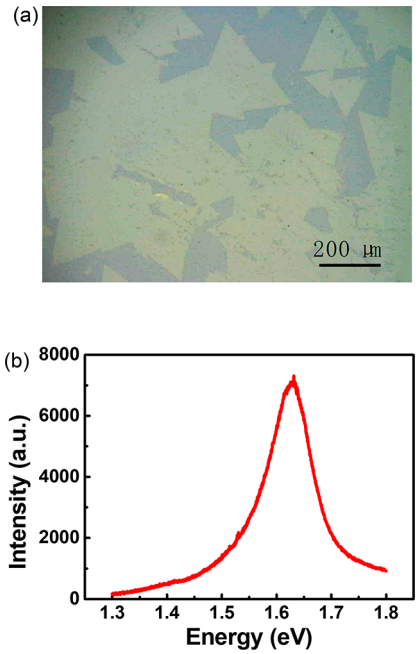

Figure 1. (a) Optical microscope image and (b) photoluminescence spectrum of CVD-grown monolayer WSe_2.

Previous studies have shown plasmonic enhancement of bulk material photocatalysts.[28,29] For example, Liu et al. showed that the addition of the plasmonic Au nanoparticles can enhance the performance of photocatalytic water splitting of bulk TiO_2 material by 66× times under visible wavelength illumination.[21] Christopher et al. showed that plasmonic nanostructures of silver can concurrently use low-intensity visible light and thermal energy to drive catalytic oxidation reactions at lower temperatures than their conventional counterparts that use only thermal stimulus.[30] Tian et al. reported photocatalytic oxidation of ethanol and methanol in nanoporous TiO_2 films exhibiting enhancement by loading with plasmonic gold and silver nanoparticles.[31] Kowalska et al. showed that gold-modified titania powders have enhanced photocatalytic activity under visible illumination, due to greater light absorption resulting from transverse and longitudinal local surface plasmon resonance of rod-like gold particles.[32]

In the work presented here, monolayer WSe_2 was grown on 90 nm of SiO_2/Si via CVD with solid precursors in a similar process to that previously shown for $MoSe_2$ monolayer growth. Approximately 100 mg of solid Se pellets were put into an alumina boat and placed into the first zone of a two-zone, 2 in. diameter quartz furnace. Another alumina boat containing 25 mg of WO_3 powder was placed 25 cm downstream from the Se source in the second, higher temperature zone of the furnace. The SiO_2/Si growth substrate was treated with hexamethyldisilazane (HMDS) and perylene-3,4,9,10 tetracarboxylic acid tetrapotassium salt (PTAS) before being placed face-down about 5 mm above the WO_3 powder. After purging with 1000 sccm of Ar for 5 min, the Se zone was heated to 500 °C and main growth zone to 900 °C. For the growth phase, a gas flow of 25 sccm Ar and 5 sccm H_2 were maintained for 30 min, after which the furnace was ramped down under inert Ar flow until cooled. Monolayer WSe_2 was then transferred from the SiO_2 growth substrate onto an indium tin oxide (ITO)-coated glass slide using a drop-casted PMMA support layer and dilute 2% HF to aid in delamination. We then evaporate a gold film with a nominal thickness of 5 nm on half of the surface of the WSe_2 monolayer using a shadow mask. This thin gold film is known to form island-like growth that is strongly plasmonic and serves as a good substrate for surface enhanced Raman spectroscopy (SERS) as well as plasmon-enhanced photochemistry.[21] An alternative method of monolayer WSe_2 growth have been added to the Supporting Information.[33−35]

Figure 2a shows an illustration of the sample geometry, where an insulated copper wire is attached to the WSe_2/ITO using silver paint and the whole sample, excluding the top surface, is encased in epoxy to insulate it from the electrolytic solution. The photoelectrochemical reaction rate obtained with this WSe_2 monolayer electrode both with and without the Au nanoislands was measured in a pH = 7, 1 M NaI solution using a three-terminal potentiostat (Gamry, Inc.) with the monolayer WSe_2 monolayer, a Ag/AgCl electrode, and a Pt wire functioning as the working, reference, and counter electrodes, respectively. Here, the iodide/iodine redox system is chosen because most redox systems oxidize the surface of WSe_2 and $MoSe_2$ to an extent that increases gradually with increasing positive redox potential. The I^-/I_2 redox couple counteracts the surface changes, suppressing the potential drop in the surface, which offer higher solar-to-electrical conversion efficiency and better stability for WSe_2 and $MoSe_2$.[36−38] An

DOI: 10.1021/acsphotonics.9b00089
ACS Photonics 2019, 6, 787−792

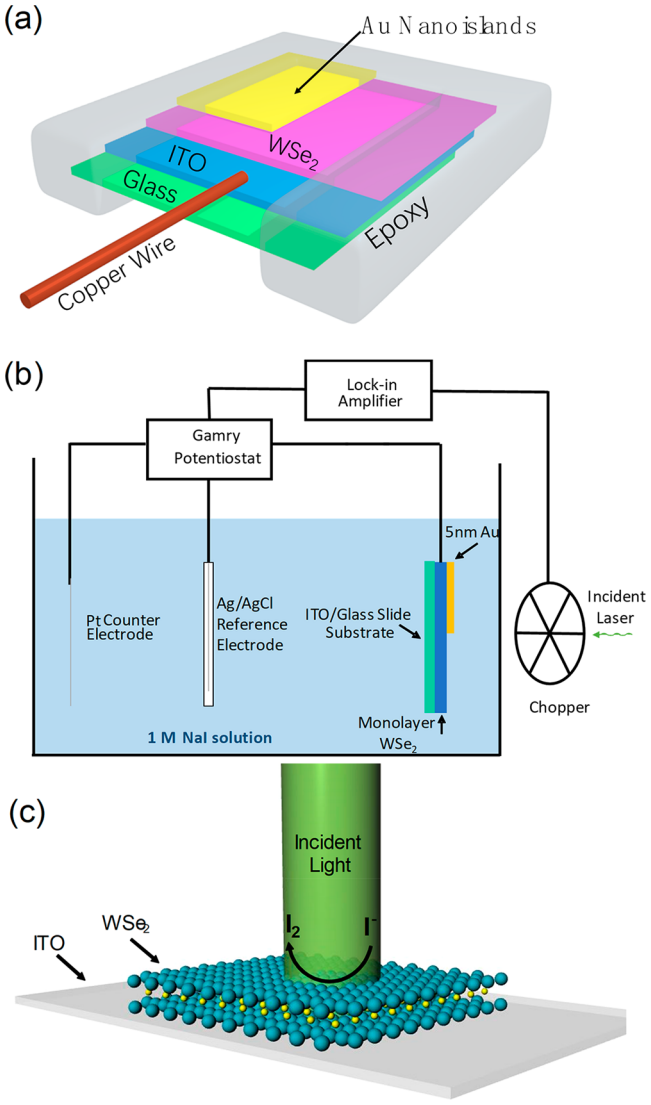

Figure 2. (a) Diagram illustrating the basic sample configuration. (b) Schematic circuit diagram of the three-terminal photoelectrochemical setup with the modulated laser and AC lock-in amplifier. (c) Schematic diagram of the photocatalytic iodine redox process.

AC lock-in technique is used to detect the very small photocurrents (nA) generated by the WSe_2 films, as illustrated in Figure 2b. The incident laser is chopped at 150 Hz by a chopper wheel (Stanford Research Systems, Model SR540) connected to the "REF IN" terminal of the lock-in amplifier (Standard Research Systems, Model SRS830 DSP), as shown in Figure S1 of the Supporting Information. This enables the lock-in amplifier to detect responses only at the specific frequency of the modulated light, providing a very sensitive measure of the photoresponse of these photocatalytic surfaces, while ignoring the DC electrochemical current. The current output of the Gamry potentiostat is connected to the input channel of the lock-in amplifier to measure the AC photoresponse from the sample at the same frequency as the chopped laser.

The DC current, AC current, and AC phase for the bare monolayer WSe_2 monolayer electrode (i.e., without Au nanoislands) without and with illumination under visible light (0.21 mW/cm^2, 532 nm) are shown in Figure 3a and b, respectively. Without illumination (Figure 3a), the WSe_2 exhibits only noise in the AC current, as expected. Under illumination (Figure 3b), however, the bare WSe_2 shows approximately an AC photocurrent of 45 nA, which is approximately 1000th of the DC current, demonstrating that our AC lock-in technique provides an extremely sensitive measure of the photoresponse from the WSe_2 photocatalytic surfaces while ignoring the purely DC electrochemical signal. Since we are irradiating monolayer WSe_2, the photocurrent is limited by the inherently small optical density of the monolayer material. As a control experiment, Figure 3c shows the same AC photocurrent measurements for bare ITO glass slide without any WSe_2. Under the same illumination conditions, this bare ITO electrode shows no photocurrent (<1 nA), verifying that the photoresponse we observed from the monolayer WSe_2 electrode is not simply originating from the underlying ITO substrate.

Figure 4 shows the photocatalytic enhancement due to the addition of the plasmonic Au nanoislands observed under 532 nm wavelength illumination (0.21 mW/cm^2). Figure 4a shows a direct comparison of the AC photocurrent taken for WSe_2 both with and without Au nanoislands. For bare WSe_2 without Au nanoparticles, a small photocurrent around 20 nA is observed. A significant enhancement in the photocurrent (7×) is evident for the WSe_2 with plasmonic Au nanoparticles, resulting in a photocurrent of 0.14 μA. The AC phase for WSe_2 both with and without Au nanoparticles are nearly identical during the measurement, as shown in Figure 4b, verifying that our signal is "locked" to the specific frequency of the modulated light.

Figure 5 shows the electromagnetic response of the Au nanoislands/monolayer WSe_2 composite film calculated using the finite difference time domain (FDTD) method. Figure 5a shows a TEM image of the gold nanoislands deposited on top of monolayer WSe_2. The dark gray regions correspond to the gold nanoislands and the light regions represent the space between. The electric field intensity distribution of this film when irradiated on resonance is shown in Figure 5b and is dominated by localized "hot spots" that occur between nearly touching Au nanoislands.[39−42] Here, the "hot spot" regions can be seen clearly between nearly touching Au nanoislands. In these local hot spot regions, the electric field intensity at the monolayer WSe_2 surface can be as much as 890× times higher than the incident electric field intensity. This means that the photon absorption rate and electron−hole pair generation rate are 3 orders of magnitude higher than that of the incident electromagnetic radiation in the brightest spots (i.e., without the Au nanoislands). It is also evident from Figure 5b that a vast majority of the photocatalytic surface is not significantly enhanced (i.e., away from the "hot spots"). We can estimate the overall plasmonic enhancement factor from these electromagnetic simulations by evaluating the following integral:

$$\mathrm{EF} = \frac{\int |E|^2 \mathrm{d}x\mathrm{d}y}{\int |E_0|^2 \mathrm{d}x\mathrm{d}y}$$

where the integral is taken over the area of the simulation window in x and y (200 μm × 200 μm). Evaluating this integral, based on the simulation results shown in Figure 5, yields an enhancement factor of 3.9×, which is consistent with our experimental observations. Figure S3 shows an average measured enhancement factor of 5.0 at 532 nm and 7.2 at 633 nm, which indicates that the plasmonic nanoislands couple 633 nm light more efficiently in the plane of the WSe_2 monolayer

DOI: 10.1021/acsphotonics.9b00089
ACS Photonics 2019, 6, 787−792

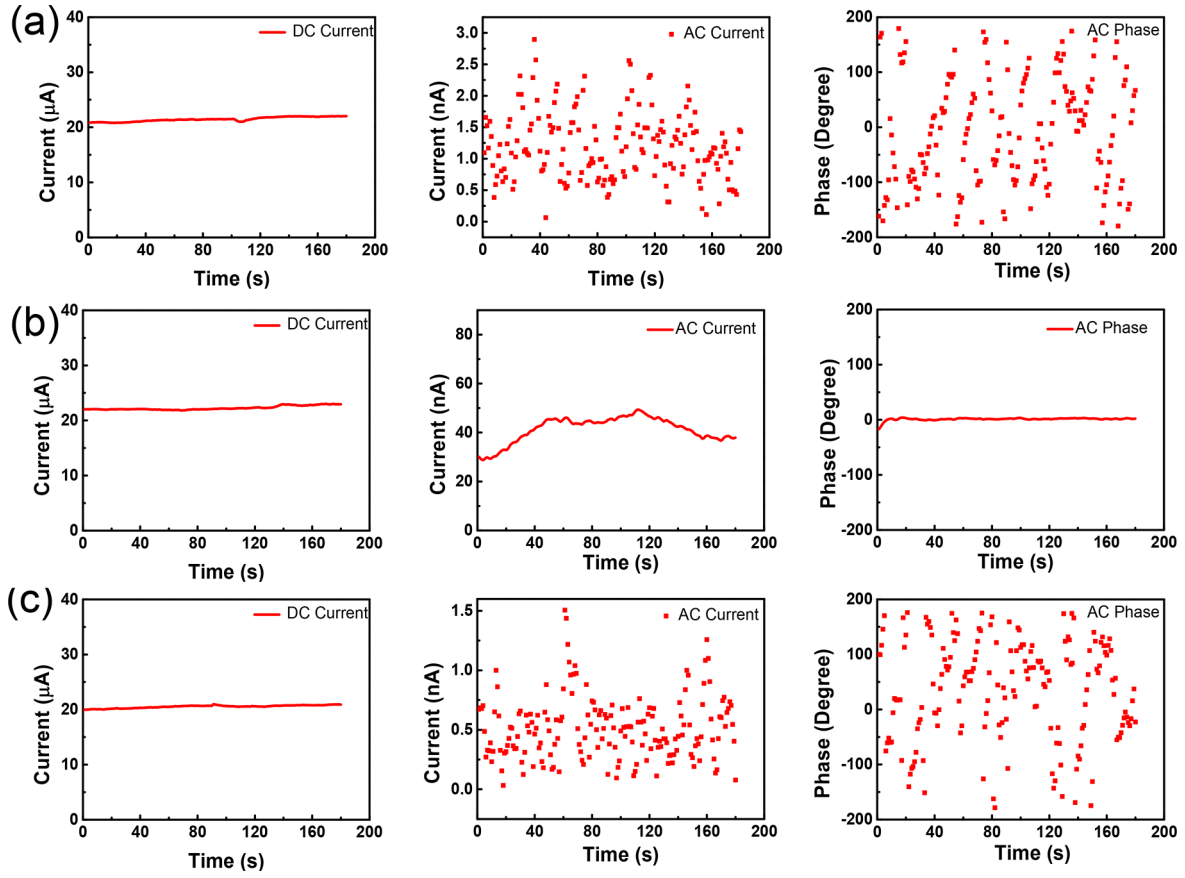

Figure 3. DC current, AC current, and AC phase measurements for the bare WSe_2 monolayer electrode (i.e., without Au nanoislands) (a) without and (b) with illumination under visible light and (c) bare ITO glass slide without WSe_2 under the same illumination conditions in (b).

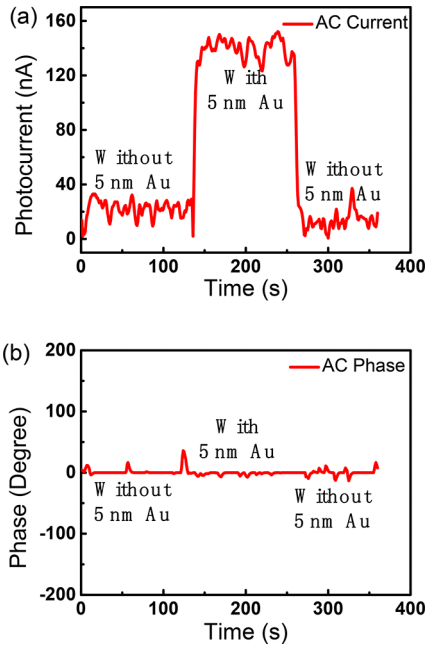

Figure 4. (a) AC photocurrent and (b) AC phase measurements for the monolayer WSe_2 electrode with and without Au nanoislands under visible illumination.

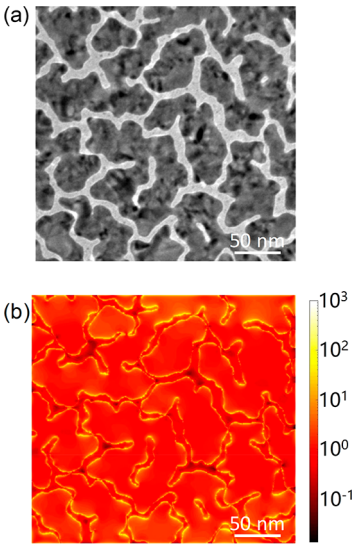

Figure 5. (a) Transmission electron microscope (TEM) image of 5 nm Au nanoisland film. (b) Enhancement factor of the electric field intensity at the Au nanoislands/monolayer WSe_2 interface calculated using the FDTD method.

than 532 nm. Figure S4 in the Supporting Information shows a calculated enhancement factor of 8.26 at 633 nm. Based on these results, we feel that we have obtained a detailed understanding of the mechanism of enhancement observed in our experimental work. In essence, these FDTD simulations show that the plasmonic nanoislands couple light very efficiently from the far field to near-field in the plane of the monolayer WSe_2 monolayer, thus improving the photoconversion efficiency.

DOI: 10.1021/acsphotonics.9b00089
ACS Photonics 2019, 6, 787−792

In conclusion, we demonstrated plasmonic enhancement of monolayer WSe_2 photocatalysis in the visible wavelength range by exploiting the surface plasmon resonance of 5 nm gold nanoislands. The addition of Au nanoparticles leads to a 7× increase in the photocurrent (from 20 nA to 0.14 μA) at a wavelength of 532 nm and improves the incident photon-to-current conversion efficiency from 3.5% to 24.7%. FDTD simulation of this process suggests that the local electric fields produced by the surface plasmons couple light efficiently to the surface of monolayer WSe_2, particularly in the local hot spot regions, thereby increasing the electron−hole pair generation rate at the surface of the WSe_2 through near-field optical enhancement. This increases the amount of photogenerated charge contributing to these photoelectrochemical reactions and presents a possible route toward improving direct solar fuel production. By integrating the electric field intensity over the entire area of our simulation window, we obtain overall enhancement factor of 3.9×, which agrees well with our experimental findings.

■ ASSOCIATED CONTENT

Supporting Information

The Supporting Information is available free of charge on the ACS Publications website at DOI: 10.1021/acsphotonics.9b00089.

Schematic of AC lock-in technique, photocurrent measurements for controlled experiment samples, wavelength-dependent and intensity-dependent on photocurrent measurement, and FDTD simulation for 633 nm (PDF)

■ AUTHOR INFORMATION

Corresponding Author

*E-mail: scronin@usc.edu.

ORCID

Wencai Ren: 0000-0003-4997-8870

Eric Pop: 0000-0003-0436-8534

Stephen B. Cronin: 0000-0001-7089-6672

Notes

The authors declare no competing financial interest.

■ ACKNOWLEDGMENTS

This research was supported by NSF Award Nos. 1512505 (J.C.) and 1708581 (H.S.), Army Research Office ARO Award No. W911NF-14-1-0228 (L.S.), and Air Force Office of Scientific Research (AFOSR) Grant No. FA9550-15-1-0184 (B.H.). The work at Stanford was supported in part by AFOSR Grant FA9550-14-1-0251 and by the NSF EFRI 2-DARE Grant 1542883. C.S.B. acknowledges support from the NSF Graduate Research Fellowship under Grant No. DGE-114747.

■ REFERENCES

(1) Walter, M. G.; Warren, E. L.; McKone, J. R.; Boettcher, S. W.; Mi, Q.; Santori, E. A.; Lewis, N. S. Solar water splitting cells. *Chem. Rev.* **2010**, *110* (11), 6446−6473.

(2) Maeda, K.; Domen, K. New non-oxide photocatalysts designed for overall water splitting under visible light. *J. Phys. Chem. C* **2007**, *111* (22), 7851−7861.

(3) Lee, J. S. Photocatalytic water splitting under visible light with particulate semiconductor catalysts. *Catal. Surv. Asia* **2005**, *9* (4), 217−227.

(4) Kudo, A.; Miseki, Y. Heterogeneous photocatalyst materials for water splitting. *Chem. Soc. Rev.* **2009**, *38* (1), 253−278.

(5) Grätzel, M. Photoelectrochemical cells. *Nature* **2001**, *414* (6861), 338.

(6) Fujishima, A.; Honda, K. Electrochemical photolysis of water at a semiconductor electrode. *Nature* **1972**, *238* (5358), 37.

(7) Sayama, K.; Mukasa, K.; Abe, R.; Abe, Y.; Arakawa, H. Stoichiometric water splitting into H_2 and O_2 using a mixture of two different photocatalysts and an IO^{3-}/I^- shuttle redox mediator under visible light irradiation. *Chem. Commun.* **2001**, No. 23, 2416−2417.

(8) Kato, H.; Hori, M.; Konta, R.; Shimodaira, Y.; Kudo, A. Construction of Z-scheme type heterogeneous photocatalysis systems for water splitting into H_2 and O_2 under visible light irradiation. *Chem. Lett.* **2004**, *33* (10), 1348−1349.

(9) Jaramillo, T. F.; Baeck, S. H.; Kleiman-Shwarsctein, A.; McFarland, E. W. Combinatorial electrochemical synthesis and screening of mesoporous ZnO for photocatalysis. *Macromol. Rapid Commun.* **2004**, *25* (1), 297−301.

(10) Zhao, Z. G.; Miyauchi, M. Nanoporous-Walled Tungsten Oxide Nanotubes as Highly Active Visible-Light-Driven Photocatalysts. *Angew. Chem., Int. Ed.* **2008**, *47* (37), 7051−7055.

(11) Abe, R.; Takata, T.; Sugihara, H.; Domen, K. Photocatalytic overall water splitting under visible light by TaON and WO_3 with an IO^{3-}/I^- shuttle redox mediator. *Chem. Commun.* **2005**, No. 30, 3829−3831.

(12) Higashi, M.; Abe, R.; Teramura, K.; Takata, T.; Ohtani, B.; Domen, K. Two step water splitting into H_2 and O_2 under visible light by $ATaO_2N$ (A= Ca, Sr, Ba) and WO_3 with IO^{3-}/I^-shuttle redox mediator. *Chem. Phys. Lett.* **2008**, *452* (1−3), 120−123.

(13) Fujishima, A.; Zhang, X.; Tryk, D. A. Heterogeneous photocatalysis: from water photolysis to applications in environmental cleanup. *Int. J. Hydrogen Energy* **2007**, *32* (14), 2664−2672.

(14) Bak, T.; Nowotny, J.; Rekas, M.; Sorrell, C. Photo-electrochemical hydrogen generation from water using solar energy. Materials-related aspects. *Int. J. Hydrogen Energy* **2002**, *27* (10), 991−1022.

(15) Liu, R.; Lin, Y.; Chou, L. Y.; Sheehan, S. W.; He, W.; Zhang, F.; Hou, H. J.; Wang, D. Water Splitting by Tungsten Oxide Prepared by Atomic Layer Deposition and Decorated with an Oxygen-Evolving Catalyst. *Angew. Chem.* **2011**, *123* (2), 519−522.

(16) Ni, M.; Leung, M. K.; Leung, D. Y.; Sumathy, K. A review and recent developments in photocatalytic water-splitting using TiO_2 for hydrogen production. *Renewable Sustainable Energy Rev.* **2007**, *11* (3), 401−425.

(17) Singh, A. K.; Mathew, K.; Zhuang, H. L.; Hennig, R. G. Computational Screening of 2D Materials for Photocatalysis. *J. Phys. Chem. Lett.* **2015**, *6* (6), 1087−98.

(18) Sun, Y.; Sun, Z.; Gao, S.; Cheng, H.; Liu, Q.; Lei, F.; Wei, S.; Xie, Y. All-Surface-Atomic-Metal Chalcogenide Sheets for High-Efficiency Visible-Light Photoelectrochemical Water Splitting. *Adv. Energy Mater.* **2014**, *4* (1), 1300611.

(19) Voiry, D.; Yamaguchi, H.; Li, J.; Silva, R.; Alves, D. C.; Fujita, T.; Chen, M.; Asefa, T.; Shenoy, V. B.; Eda, G.; Chhowalla, M. Enhanced catalytic activity in strained chemically exfoliated WS(2) nanosheets for hydrogen evolution. *Nat. Mater.* **2013**, *12* (9), 850−5.

(20) Liang, L.; Sun, Y.; Lei, F.; Gao, S.; Xie, Y. Free-floating ultrathin tin monoxide sheets for solar-driven photoelectrochemical water splitting. *J. Mater. Chem. A* **2014**, *2* (27), 10647.

(21) Liu, Z.; Hou, W.; Pavaskar, P.; Aykol, M.; Cronin, S. B. Plasmon resonant enhancement of photocatalytic water splitting under visible illumination. *Nano Lett.* **2011**, *11* (3), 1111−6.

(22) Qiu, J.; Zeng, G.; Pavaskar, P.; Li, Z.; Cronin, S. B. Plasmon-enhanced water splitting on TiO_2-passivated GaP photocatalysts. *Phys. Chem. Chem. Phys.* **2014**, *16* (7), 3115−3121.

(23) Hou, W.; Liu, Z.; Pavaskar, P.; Hung, W. H.; Cronin, S. B. Plasmonic enhancement of photocatalytic decomposition of methyl orange under visible light. *J. Catal.* **2011**, *277* (2), 149−153.

DOI: 10.1021/acsphotonics.9b00089
ACS Photonics 2019, 6, 787−792

(24) Gomez, L.; Sebastian, V.; Arruebo, M.; Santamaria, J.; Cronin, S. B. Plasmon-enhanced photocatalytic water purification. *Phys. Chem. Chem. Phys.* **2014**, *16* (29), 15111−15116.
(25) Hou, W.; Hung, W. H.; Pavaskar, P.; Goeppert, A.; Aykol, M.; Cronin, S. B. Photocatalytic conversion of CO_2 to hydrocarbon fuels via plasmon-enhanced absorption and metallic interband transitions. *ACS Catal.* **2011**, *1* (8), 929−936.
(26) Chien, T.-m.; Pavaskar, P.; Hung, W. H.; Cronin, S.; Chiu, S.-H.; Lai, S.-N. Study of the plasmon energy transfer processes in dye sensitized solar cells. *J. Nanomater.* **2015**, *2015*, 2.
(27) Hou, W.; Pavaskar, P.; Liu, Z.; Theiss, J.; Aykol, M.; Cronin, S. B. Plasmon resonant enhancement of dye sensitized solar cells. *Energy Environ. Sci.* **2011**, *4* (11), 4650−4655.
(28) Wu, N. Plasmonic metal−semiconductor photocatalysts and photoelectrochemical cells: a review. *Nanoscale* **2018**, *10* (6), 2679−2696.
(29) DuChene, J. S.; Sweeny, B. C.; Johnston-Peck, A. C.; Su, D.; Stach, E. A.; Wei, W. D. Prolonged hot electron dynamics in plasmonic-metal/semiconductor heterostructures with implications for solar photocatalysis. *Angew. Chem., Int. Ed.* **2014**, *53* (30), 7887−7891.
(30) Christopher, P.; Xin, H.; Linic, S. Visible-light-enhanced catalytic oxidation reactions on plasmonic silver nanostructures. *Nat. Chem.* **2011**, *3* (6), 467.
(31) Tian, Y.; Tatsuma, T. Plasmon-induced photoelectrochemistry at metal nanoparticles supported on nanoporous TiO_2. *Chem. Commun. (Cambridge, U. K.)* **2004**, No. 16, 1810−1.
(32) Kowalska, E.; Mahaney, O. O.; Abe, R.; Ohtani, B. Visible-light-induced photocatalysis through surface plasmon excitation of gold on titania surfaces. *Phys. Chem. Chem. Phys.* **2010**, *12* (10), 2344−55.
(33) Gao, L.; Ren, W.; Xu, H.; Jin, L.; Wang, Z.; Ma, T.; Ma, L.-P.; Zhang, Z.; Fu, Q.; Peng, L.-M. Repeated growth and bubbling transfer of graphene with millimetre-size single-crystal grains using platinum. *Nat. Commun.* **2012**, *3*, 699.
(34) Gao, Y.; Liu, Z.; Sun, D.-M.; Huang, L.; Ma, L.-P.; Yin, L.-C.; Ma, T.; Zhang, Z.; Ma, X.-L.; Peng, L.-M. Large-area synthesis of high-quality and uniform monolayer WS_2 on reusable Au foils. *Nat. Commun.* **2015**, *6*, 8569.
(35) Gao, Y.; Hong, Y. L.; Yin, L. C.; Wu, Z.; Yang, Z.; Chen, M. L.; Liu, Z.; Ma, T.; Sun, D. M.; Ni, Z.; Ma, X. L.; Cheng, H. M.; Ren, W. Ultrafast Growth of High-Quality Monolayer WSe_2 on Au. *Adv. Mater.* **2017**, *29* (29), 1700990.
(36) Tributsch, H. Electrochemical solar cells based on layer-type transition metal compounds: Performance of electrode material. *Sol. Energy Mater.* **1979**, *1* (3−4), 257−269.
(37) Kline, G.; Kam, K.; Canfield, D.; Parkinson, B. Efficient and stable photoelectrochemical cells constructed with WSe_2 and $MoSe_2$ photoanodes. *Sol. Energy Mater.* **1981**, *4* (3), 301−308.
(38) Kam, K.; Parkinson, B. Detailed photocurrent spectroscopy of the semiconducting group VIB transition metal dichalcogenides. *J. Phys. Chem.* **1982**, *86* (4), 463−467.
(39) Pavaskar, P.; Cronin, S. B. Iterative optimization of plasmon resonant nanostructures. *Appl. Phys. Lett.* **2009**, *94* (25), 253102.
(40) Pavaskar, P.; Hsu, I.-K.; Theiss, J.; Hsuan Hung, W.; Cronin, S. B. A microscopic study of strongly plasmonic Au and Ag island thin films. *J. Appl. Phys.* **2013**, *113* (3), 034302.
(41) Theiss, J.; Pavaskar, P.; Echternach, P. M.; Muller, R. E.; Cronin, S. B. Plasmonic nanoparticle arrays with nanometer separation for high-performance SERS substrates. *Nano Lett.* **2010**, *10* (8), 2749−2754.
(42) Theiss, J.; Aykol, M.; Pavaskar, P.; Cronin, S. B. Plasmonic mode mixing in nanoparticle dimers with nm-separations via substrate-mediated coupling. *Nano Res.* **2014**, *7* (9), 1344−1354.

DOI: 10.1021/acsphotonics.9b00089
ACS Photonics 2019, 6, 787−792

Supplemental Information for

Plasmon-Resonant Enhancement of Photocatalysis on Monolayer WSe_2

Jihan Chen[1], Connor S. Bailey[2], Yilun Hong[3,4], Li Wang[5], Zhi Cai[6], Lang Shen [6], Bingya Hou[1], Yu Wang[6], Haotian Shi[7], Justin Sambur[5], Wencai Ren[3,4], Eric Pop[2] and Stephen B. Cronin[1,7,8]

[1]Ming Hsieh Department of Electrical Engineering, [6]Mork Family Department of Chemical Engineering and Materials Science, [7]Department of Chemistry, [7]Department of Physics and Astronomy, University of Southern California, Los Angeles, CA 90089, USA

[2]Department of Electrical Engineering, Stanford University, Stanford, CA 94305, USA

[3]Shenyang National Laboratory for Materials Science, Institute of Metal Research, Chinese Academy of Sciences, Shenyang, 110016, P. R. China

[4]School of Materials Science and Engineering, University of Science and Technology of China, 72 Wenhua Road, Shenyang, 110016, P. R. China

[5]Department of Chemistry, Colorado State University, Fort Collins, CO, 80523, USA

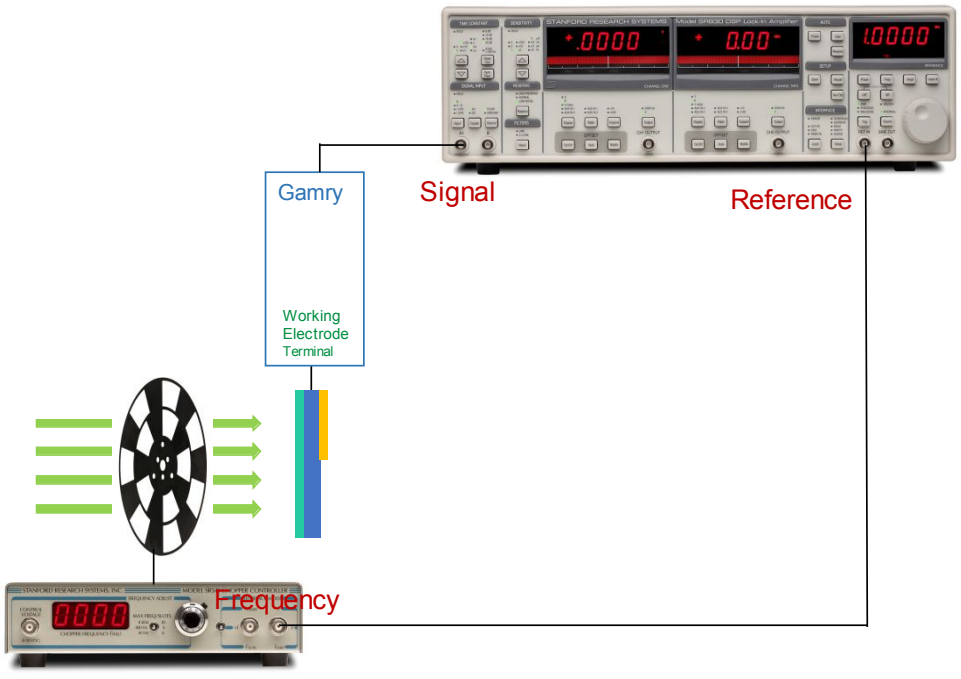

Figure S1. Schematic circuit diagram of the AC lock-in technique, in which the incident light is modulated by a chopper wheel and chopper controller, which provides a reference signal for the lock-in amplifier. This enables the lock-in amplifier to detect only voltages at the specific

frequency of the modulated light, providing a very sensitive measure of the photoresponse of these photocatalytic surfaces.

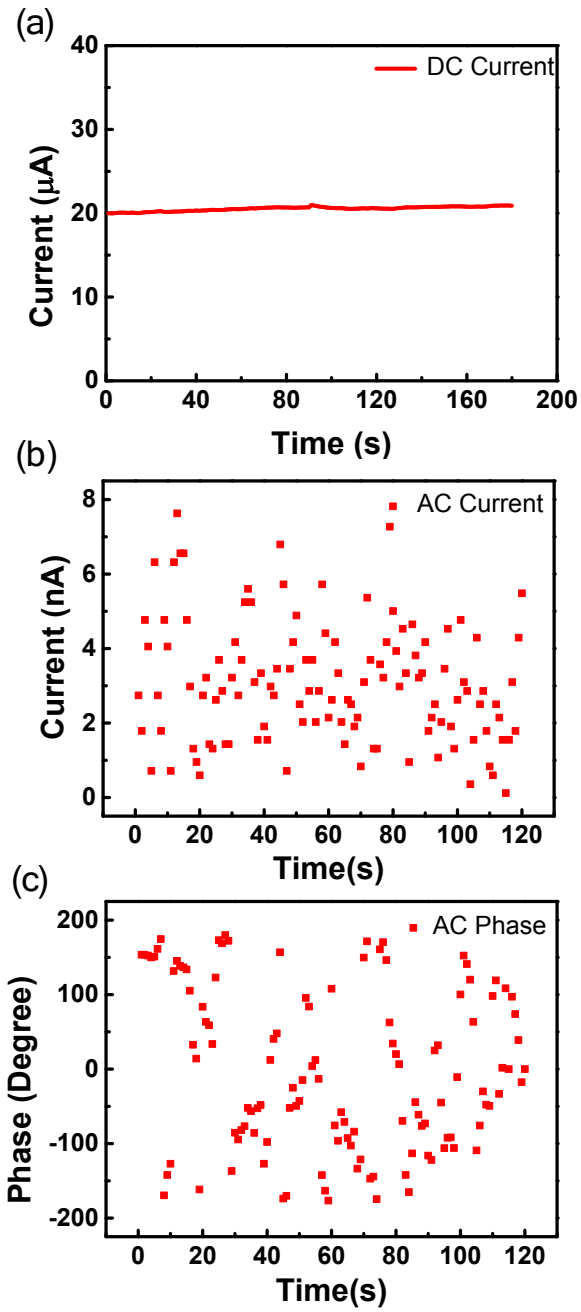

Figure S2. (a) DC current, (b) AC current, and (c) AC phase measurements for the ITO electrode with only 5nm Au nanoislands without WSe_2.

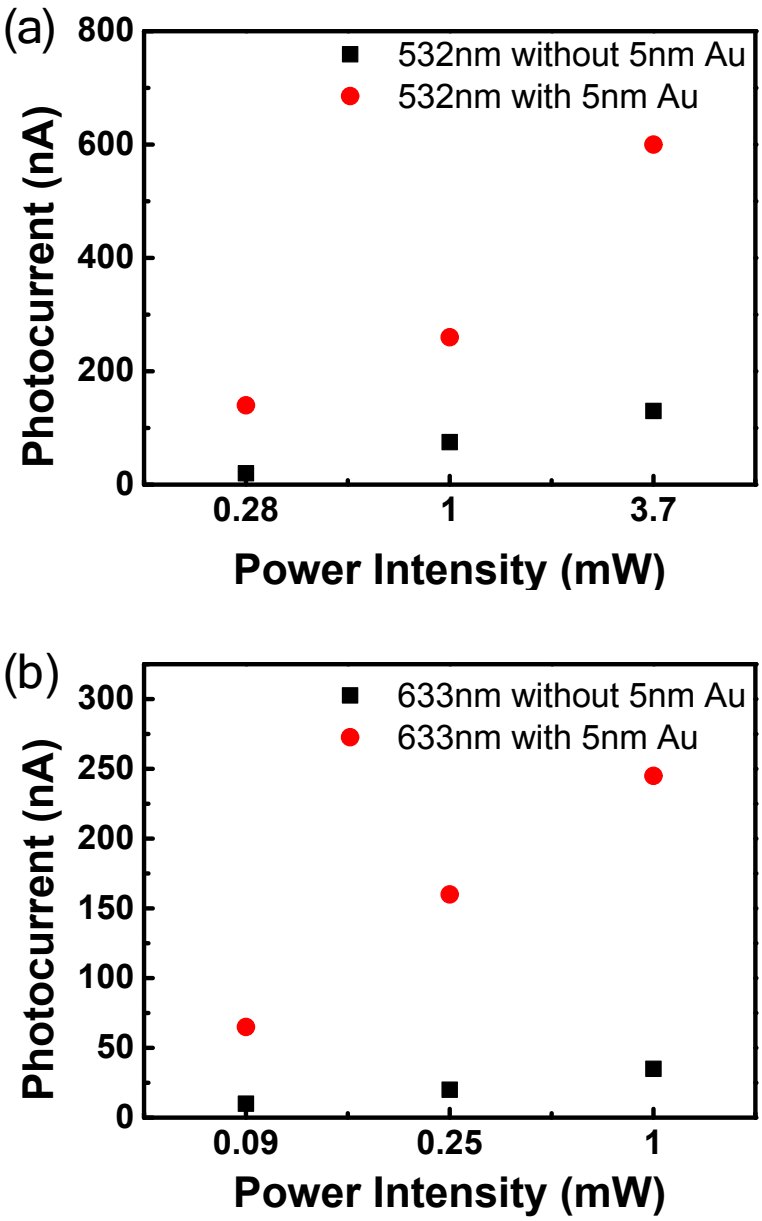

Figure S3. (a) Intensity dependent of photocurrent measurement for 532 nm wavelength (b) Intensity dependent of photocurrent measurement for 633 nm wavelength.

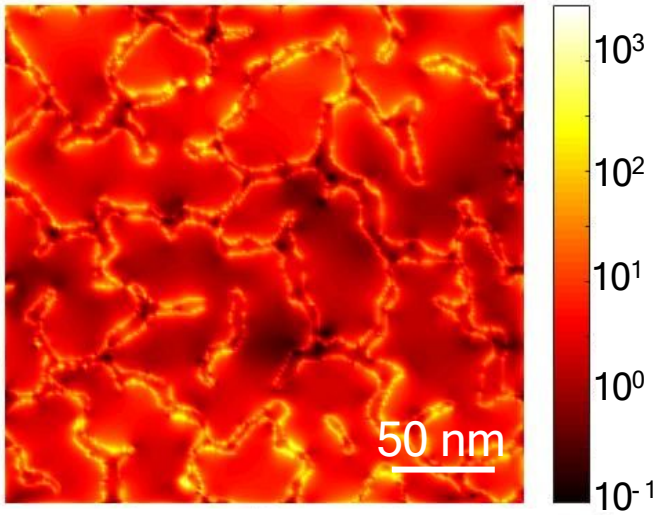

Figure S4. Enhancement factor of the electric field intensity at the Au-WSe_2 interface for 633 nm wavelength calculated using the FDTD method.

An alternative growth method of monolayer WSe_2: WSe_2 was grown on gold foil by ambient-pressure CVD with solid precursors[1], which is similar to that previously shown for WS_2 monolayer growth.[1-2] A piece of polycrystalline Au foil was first finely polished and annealed, and then placed in a small quartz boat together with 100 mg WO_3 powder upstream, loaded at the reaction zone of a horizontal CVD furnace equipped with a 1-inch-diameter quartz tube. Another small quartz boat containing 1000 mg Se pellets was placed upstream at the low temperature zone of the furnace. After the reaction zone was heated to 900 °C in an argon atmosphere (100 s.c.c.m.), a small flow rate of H_2 (0.5 s.c.c.m.) was introduced to initiate WSe_2 growth. After several minutes, we rapidly stopped the growth by quickly moving the two boats to low-temperature zone. Monolayer WSe_2 was then transferred from the gold foil onto an indium tin oxide (ITO)-coated glass slide by electrochemical bubbling transfer method using a drop-casted PMMA support layer.[1, 3]

Reference

1. Gao, Y.; Hong, Y. L.; Yin, L. C.; Wu, Z.; Yang, Z.; Chen, M. L.; Liu, Z.; Ma, T.; Sun, D. M.; Ni, Z.; Ma, X. L.; Cheng, H. M.; Ren, W., Ultrafast Growth of High-Quality Monolayer WSe_2 on Au. *Adv Mater* **2017,** *29* (29).
2. Gao, Y.; Liu, Z.; Sun, D.-M.; Huang, L.; Ma, L.-P.; Yin, L.-C.; Ma, T.; Zhang, Z.; Ma, X.-L.; Peng, L.-M., Large-area synthesis of high-quality and uniform monolayer WS_2 on reusable Au foils. *Nature communications* **2015,** *6*, 8569.
3. Gao, L.; Ren, W.; Xu, H.; Jin, L.; Wang, Z.; Ma, T.; Ma, L.-P.; Zhang, Z.; Fu, Q.; Peng, L.-M., Repeated growth and bubbling transfer of graphene with millimetre-size single-crystal grains using platinum. *Nature communications* **2012,** *3*, 699.